Journal of
Applied Crystallography
ISSN 0021-8898

Received 16 August 2006
Accepted 1 February 2007

Anomalous grazing-incidence small-angle X-ray scattering investigation on the surface morphology of an FePt magnetic nanoparticle monolayer on functional modulated substrates

Tzu-Wen Huang,[a] Kuan-Li Yu,[b] Yen-Fa Liao[a] and Chih-Hao Lee[a,c]*

[a]Department of Engineering and System Science, National Tsing-Hua University, Hsinchu, Taiwan, [b]National Synchrotron Radiation Research Center, Hsinchu, Taiwan, and [c]Nuclear Science and Technology Development Center, National Tsing-Hua University, Hsinchu, Taiwan. Correspondence e-mail: chlee@mx.nthu.edu.tw

The structural stability and coalescence of self-assembled FePt monolayer nanoparticles on functional substrates with/without an Au overlayer during annealing were studied. From X-ray diffraction and the anomalous grazing-incidence small-angle X-ray scattering techniques, the nanoparticles were found to be intact under the annealing process when a 5–10 nm overlayer of Au was deposited on top of FePt monolayer nanoparticles. From the simulation result, the particle size 4.5 $\pm$ 0.5 nm is typically unchanged, but the distance between particles is reduced from 7.5 $\pm$ 1.5 nm to 5.5 $\pm$ 1.1 nm after annealing. The results suggest that the 5 nm Au coverlayer is an effective diffusing barrier layer to prevent the FePt nanoparticles from sintering during the annealing process.

1. Introduction

Since a well ordered self-assembled FePt nanoparticle system was synthesized by Sun *et al.* (2000), recent attention has shifted to fabricate a monolayer of magnetic nanoparticles due to their potential application in an ultra-high density recording system. To deposit a monolayer of particles under control, the functional substrates such as polyethylenimine (PEI) or [3-(2-aminoethylamino)propyl] trimethoxysilane (APTS) were used successfully (Sun *et al.*, 2003; Yu *et al.*, 2003; Huang *et al.*, 2006). However, due to the limited ordering orientation of those polymers, the original well ordered self-organized behaviour of the nanoparticles system was destroyed and the stacking condition of those particles on the surface was not compact any more. Even though the functional molecules could play as a linking role in combining the silicon dioxide and the surfactants on the particle surface exactly at room temperature, the aggregation behaviour still occurs after a post annealing process caused by the burn away of the functional molecules and surfactant molecules (Huang *et al.*, 2006). The carbon existing on the particle surface produced from the burn away of surfactant might form a barrier to hinder the metal atoms on the particle surface from diffusing and sintering together (Held *et al.*, 2004). This concept of barrier behaviour caused by a heterogeneous material between particles has been achieved in immiscibility systems. For example, the gold or silver, as a coverlayer on the FePt nanoparticles, can be used to prevent the aggregation behaviour during the annealing process (Huang *et al.*, 2006). In addition, for the application of high density magnetic disk, the Au overlayer usually induces a pinning effect on the magnetic moment rotation, so that the exchange integral between each particle can be reduced to fit the demand of higher density. However, due to the heavier electron density of gold and similar lattice constant with FePt, the morphology of this nanoparticle underlayer is difficult to be observed by X-ray diffraction and scanning electron microscopy. Therefore, in this work, anomalous grazing-incidence small-angle X-ray scattering (anomalous GISAXS) was used to characterize the morphology of the FePt monolayer system with an Au coverlayer before and after the annealing process.

2. Experimental and characterization methods

2.1. Experimental procedure

FePt nanoparticles were thermally deposited by mixing two precursors, platinum acetyl acetonate and iron pentacarbonyl, in the presence of oleic acid and oleylamine stabilizers at 573 K (Huang *et al.*, 2006; Held *et al.*, 2004; Huang *et al.*, 2004; Sun *et al.*, 2000). Different particle sizes of as-synthesized FePt nanoparticles were controlled by different ratios of surfactants and precursors. Their size was measured by transmission electron microscopy (TEM) and small-angle X-ray scattering (SAXS). The composition ratio of Fe to Pt is about 48:52 which was verified by energy dispersive spectroscopy. The SAXS data were fitted by a model of core-shell structure. The inner FePt diameter can be controlled from 2.88 to 4.5 nm. The outside shell surfactant thickness was about 1.0 nm.

To prepare the PEI or APTS functional substrate, an Si(111) wafer cleaned by standard RCA (Radio Corporation of America) process was immersed into a 0.1 *M* PEI or APTS solution which was dissolved in the chloroform or alcohol for 20 h. The extra PEI or APTS molecules on the functional substrate were washed away by chloroform or alcohol. Then the sample was dried at 323 K in nitrogen and immersed into hexane dispersed with FePt nanoparticles for 1 h (Huang *et al.*, 2004). Finally, the sample was washed by hexane to remove extra nanoparticles. The X-ray reflectivity confirmed that one layer of FePt nanoparticles was formed.

1–10 nm of Au or Ag coverlayer was then deposited on the FePt monolayer by e-gun evaporation deposition under an ultra-high vacuum system to maintain the self-assembled structure. Then, the rapid thermal annealing process was carried out at 773, 873, 973 and

1073 K under a nitrogen atmosphere of 10^{-3} mbar to study the annealing effect. The surface morphology was measured by scanning electron microscopy (SEM). The X-ray diffraction (XRD) and X-ray absorption near-edge structure experiments were also performed. The X-ray measurements were done at wiggler beamlines 17B, 17C and 20A of National Synchrotron Radiation Research Center (NSRRC), Taiwan, and at the BL12B2 beamline of SPring8, Japan. The particle sizes and their dispersions on the functional substrates covered with Au were determined by anomalous GISAXS at the NSRRC.

2.2. Anomalous grazing-incidence small-angle X-ray scattering

In this system, anomalous SAXS at grazing-incidence angle was applied to measure the particle size and the inter-particle distance of the Au over monolayer FePt nanoparticles. With anomalous GISAXS, the scattering contribution from the coverlayer and background can be subtracted. The contrast variation experiment was performed at two X-ray energies, namely E_1 = 11 keV and E_2 = 11.2 keV, near the Pt$L_{\rm III}$ [$E(L_{\rm III})$ = 11.564 keV] absorption edge.

The principle of anomalous SAXS measurements has been developed by several groups (Wen *et al.*, 2005; Hindle *et al.*, 2005; Haubold *et al.*, 1996). We adopt a low-concentration case, and an ensemble of uniform FePt particles in a negligible matrix to correct the anomalous factor. The particle scattering intensity from the scattering volume, V, can be written as:

$$\frac{{\rm d}\Sigma}{{\rm d}\Omega}(Q) = C_0 n^2 f_0^2 \Phi^2(Q) V^2, \tag{1}$$

where C_0 is the number density of the particles, n is the number density of the atoms within a particle, f_0 is the average scattering amplitude which includes $f_{\rm Pt}$ and $f_{\rm Fe}$ modelling under an FePt alloy face-centred cubic structure and $\Phi^2(Q)$ is the particle form factor as functions of scattering vector Q. The scattering vector is defined by $4\pi\sin(\theta/2)/\lambda$, where θ is the scattering angle.

For a spherical particle of radius R_0, the particle form factor can be given by

$$\Phi(Q) = 3\frac{\sin(QR_0) - QR_0\cos(QR_0)}{(QR_0)^3} V_0(R_0), \tag{2}$$

where $V_0(R_0)$ is the particle volume. For a two-phase model including FePt and an Au overlayer, the total differential cross-section is given by

$$\frac{{\rm d}\Sigma}{{\rm d}\Omega}(Q) = C_0(n_{\rm p} f_{\rm p} - n_{\rm m} f_{\rm m})^2 \Phi^2(Q) V^2 + \frac{{\rm d}\Sigma}{{\rm d}\Omega_{\rm bg}}(Q), \tag{3}$$

where $n_{\rm p}$, $f_{\rm p}$, $n_{\rm m}$, and $f_{\rm m}$ are the number densities and atomic form-factors of the particles (p) and the surrounding matrix (m), respectively. In addition to the particle scattering, a background scattering term ${\rm d}\Sigma/{\rm d}\Omega_{\rm bg}(Q)$ contributes to the total differential cross-section. This background usually originates from inhomogeneities in the matrix, which can be described to be proportional to Q^{-4} in most transmission small-angle scattering experiments.

The SAXS intensity almost always contains complicated information from the matrix if the experiment is performed at one incident energy only. The contrast variation experiments running at more than two different energies near the absorption edge can be performed to separate the scattering contributed from the matrix background. Fig. 1 shows the $f'(E)$ changes at absorption edges. The atomic form factors of the FePt particles vary significantly at energies close to the Pt absorption edge, while the $f'(E)$ of the matrix remains more or less constant.

A simple subtraction of two SAXS curves measured at two different energies E_1 and E_2 near the Pt L-absorption edge results in a scattering contribution of FePt particles expressed as follows:

$$\frac{{\rm d}\Sigma}{{\rm d}\Omega_{\rm p}}(Q) = \frac{{\rm d}\Sigma}{{\rm d}\Omega}(Q, E_1) - \frac{{\rm d}\Sigma}{{\rm d}\Omega}(Q, E_2) = C_0 n^2 [f_0^2(E_1) - f_0^2(E_2)]^2 \Phi^2(Q) V^2 \times \left\{1 - \frac{2n_{\rm m} f_{\rm m}}{n\left[f_0(E_1) + f_0(E_2)\right]}\right\}. \tag{4}$$

Then, the equation can be simplified as:

$$\frac{{\rm d}\Sigma}{{\rm d}\Omega_{\rm p}}(Q) = \Delta\rho^2 \Phi^2(Q) V^2$$
$$\Delta\rho^2 = C_0 \Delta (nf)^2 \left\{1 - \frac{2n_{\rm m} f_{\rm m}}{n\left[f_0(E_1) + f_0(E_2)\right]}\right\}, \tag{5}$$

where $\Delta\rho^2$ can be considered as a scattering contrast correction term.

Then, with a local monodispersive approximation, to model the anomalous GISAXS scattering curves, the scattering cross section, $\frac{{\rm d}\hat{\sigma}}{{\rm d}\Omega}(Q)$, can be written as:

$$\frac{{\rm d}\hat{\sigma}}{{\rm d}\Omega}(Q) = \Delta\rho \int_0^\infty N(D) \left[\int_0^\infty \Phi(Q, R_{||}) N(R_{||}) S(Q, R_{||}, D)\, {\rm d}R_{||}\right] {\rm d}D, \tag{6}$$

where $\Delta\rho$ is defined in equation (5) and $\Phi(Q)$ is the form factor of a particle which is defined in equation (2). $R_{||}$ is the radius of nanoparticles along the in-plane direction and $S(Q,R_{||},D)$ is the inter-particle structure factor which will be described later.

In equation (6), $N(D)$ is the distribution of the surface to surface distance D between particles, which can be modelled by a Gaussian distribution

$$N(D) = \frac{1}{\sqrt{2\pi}\sigma_{\rm g}} \exp\left[-\frac{1}{2\sigma_{\rm g}^2}(D - D_0)^2\right], \tag{7}$$

In addition, the size distribution of the FePt nanoparticles $N(R)$ is described as a log-normal distribution,

$$N(R) = \frac{1}{\sqrt{2\pi}\sigma R} \exp\left[-\frac{1}{2\sigma^2} \ln^2\left(\frac{R}{R_0}\right)\right], \tag{8}$$

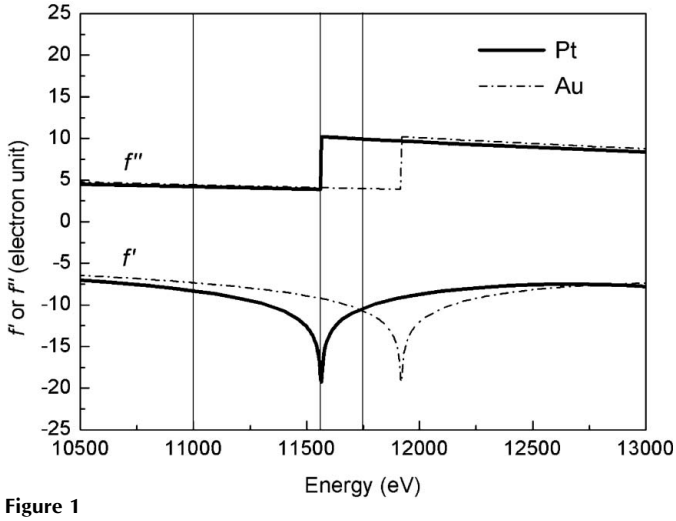

Figure 1
Anomalous correction f' and f'' for Pt and Au in the vicinity of the $L_{\rm III}$ absorption edges.

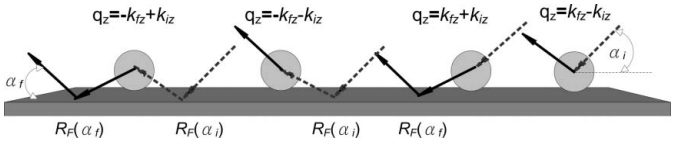

Figure 2
The four terms involved in the scattering by a supported island. The first term corresponds to a simple Born approximation.

where σ is the standard deviation of the size distribution obtained from TEM images.

To define the $S(Q,R_{||}, D)$ in equation (6) for a homogeneous and isotropic sample, we assumed that the pair correlation function and the interference function depend only on the modulus $r_{||}$ (the elementary surface area around $r_{||}$) and $Q_{||}$. Thus, in a two-dimensional system, the structure factor can be defined as:

$$S(Q_{||}) = 1 + \rho_s \int \left[g(r_{||}) - 1\right] \exp(-ir_{||}Q_{||}) \mathrm{d}^2 r_{||}, \tag{9}$$

where ρ_s is the particle density per unit surface and the pair correlation function, $g(r)$, was described under the assumption of the Debye hard core model with a power-law correction as shown in the following equations:

$$\begin{aligned} g(r) &= 0 \quad \text{for} \quad 0 \le r \le R_0 \\ g(r) &= 1 + \frac{\omega}{r^3} \quad \text{for} \quad R_0 \le r \le \infty, \end{aligned} \tag{10}$$

where ω is a constant parameter which can be found through the conservation of the number of particles (Guinier, 1963).

In the grazing-incidence geometry, with the additional reflection from the substrate and α_i (incident angle) being so close to the critical angle α_c of the total external reflection, the Born approximation has to be modified in order to account for reflection-refraction effect at the surface of the substrate. Distorted-wave Born approximation (DWBA) is considered here, rather than using the first order perturbation induced by the island roughness on the substrate surface or contrast variation to correct the unperturbed wave. A physical picture of the calculation (Rauscher *et al.*, 1999) for the scattering cross section in the DWBA with an island system is depicted in Fig. 2, where k_i and k_f are the incident and outgoing wavevectors, respectively. There are four terms involved in the scattering process associated with different scattering events involving or not involving a reflection of either the incident beam or the final beam collected on the detector. These waves interfere coherently and give rise to the following effective form factor where the classical form factor comes into play with specific momentum transfers:

$$\begin{aligned} \Phi(Q_{||}, k_{iz}, k_{fz}) = \Phi(Q_{||}, k_{fz} - k_{iz}) + R_F(\alpha_i)\Phi(Q_{||}, k_{fz} + k_{iz}) + \\ R_F(\alpha_f)\Phi(Q_{||} - k_{fz} - k_{iz}) + R_F(\alpha_i)R_F(\alpha_f)\Phi(Q_{||}, -k_{fz} + k_{iz}). \end{aligned} \tag{11}$$

Finally, if the incident beam has a finite divergence [distribution on $(2\theta_i, \alpha_i)$] and wavelength resolution, for each scattering directions $(2\theta_f, \alpha_f)$, one has to perform an incoherent sum of the intensity scattered on each plane wave:

$$\frac{\mathrm{d}\tilde{\sigma}}{\mathrm{d}\Omega}(Q) = \int_\lambda \int_\theta \int_\alpha \frac{\mathrm{d}\hat{\sigma}}{\mathrm{d}\Omega}(Q, \lambda, 2\theta, \alpha) n(\lambda) n(2\theta) n(\alpha)\, \mathrm{d}\alpha \mathrm{d}\theta \mathrm{d}\lambda. \tag{12}$$

3. Results and discussion

Fig. 3 shows the particle sizes measured both by X-ray scattering and TEM. The result shows that the particle sizes were proportional to the logarithmic molecular ratio of surfactants including oleic acid and oleylamine to Pt $(acac)_2$ precursors. This relationship which can be described as an Arrhenius rate equation might indicate that the particle sizes were controlled by the density of nucleation centres since the growth temperature and time are important controlled factors. As the total amount of surfactants increases, the activation energy of the nucleation process will increase, which is caused by the atoms migrated in a more complex solution. Hence, a lower nucleation number with higher concentrations of surfactants in the growth solution will result in a larger particle size with the same amount of precursors, under the complete reduction process.

Fig. 4 shows the XRD data of monolayer FePt nanoparticles on PEI and APTS functional substrates without an Au overlayer at

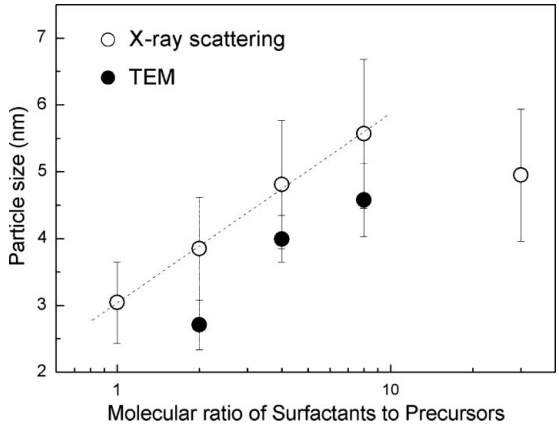

Figure 3
The result of particle size determined by X-ray scattering (open circle) and TEM (solid circle) at different molecular ratios of surfactants to precursors.

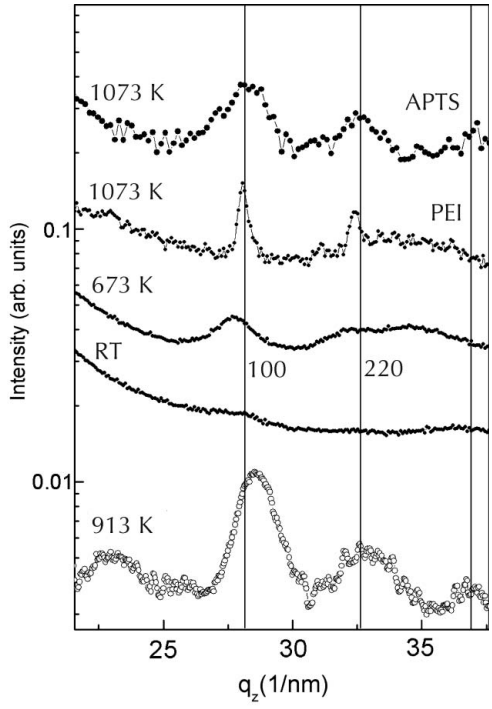

Figure 4
The XRD spectra of a monolayer of FePt nanoparticles on a functional PEI or APTS substrate under different annealing temperatures. For comparison, the XRD of a 130 nm film of FePt nanoparticles annealed at 913 K is also shown at the bottom (open circle). Two vertical lines indicate the positions of two major FePt diffraction peaks, (100) and (220).

different annealing conditions. On the PEI functional substrate, a shift of the FePt(111) diffraction peak indicates that the structure of FePt nanoparticles was transferred from an fcc phase to an $L1_0$ phase after 1073 K annealing. The coherent length of FePt nanoparticles calculated by the Scherrer formula is 4.5 ± 0.3 nm (as synthesized) and 15.1 ± 0.5 nm (after annealing). It shows that the nanoparticles aggregated even when their initial sites were pinned by PEI molecules. A similar result was also shown on the APTS, except that the coherent length of FePt nanoparticles on the APTS (7.6 ± 0.5 nm) is smaller than the one on PEI at the same annealing condition. This result may indicate that the remaining silicon atoms, which came from the burning away of the ATPS layer, exist between each particle and hinder the sintering behaviour. Another point worth noticing is that even through the self-assembled molecule, APTS, which can form a complete and smooth, flat surface at the beginning, the self-assembled phenomenon of FePt particles on the top surface was also destroyed after annealing. The surface morphology of FePt nanoparticles on the functional APTS was shown in Fig. 5.

Since the heterogeneous material, such as silicon, might become an essential factor to prevent the aggregation behaviour during the annealing, the annealing process also can be carried out on an Au covered FePt nanoparticles monolayer system. However, the XRD data show no FePt diffraction peak detectable after high temperature annealing. This possibly indicates that those FePt nanoparticles are not aggregated and the sizes are still too small to be detected under the strong diffraction background of the Au matrix. The SEM image also shows that the Au overlayer aggregates and grows into a larger domain, which is consistent with the XRD result. However, the particle size of FePt nanoparticles after the annealing process cannot be observed from the SEM image which is also due to the Au matrix.

In order to further verify the particle integrity of FePt nanoparticles after 1073 K annealing, a GISAXS experiment was performed. The GISAXS scattering intensity was analyzed following the method mentioned in §2.2. The result indicates that the characteristic size of the nanoparticle becomes larger after adding the Au overlayer both before and after annealing (Huang *et al.*, 2006). From both the GISAXS and XRD results, the particle distribution after annealing was hard to be determined. The gold with heavier electron density dominates the scattering intensity. In addition, due to the similar electron density between the Au and FePt, the use of the GISAXS technique alone cannot distinguish the morphology of FePt nanoparticles from the Au matrix. Thus, anomalous GISAXS provides exclusively the platinum information which comes from the FePt nanoparticle.

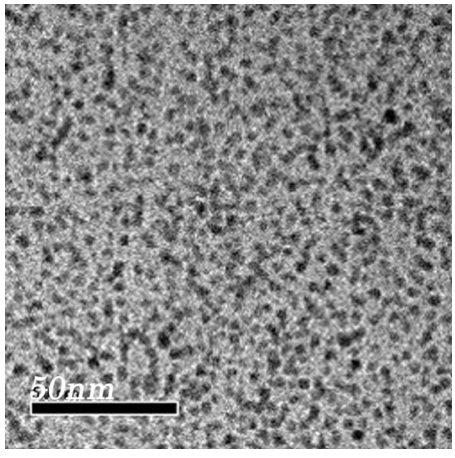

Figure 5
The surface morphology of FePt nanoparticles on the functional APTS self assembled molecular film.

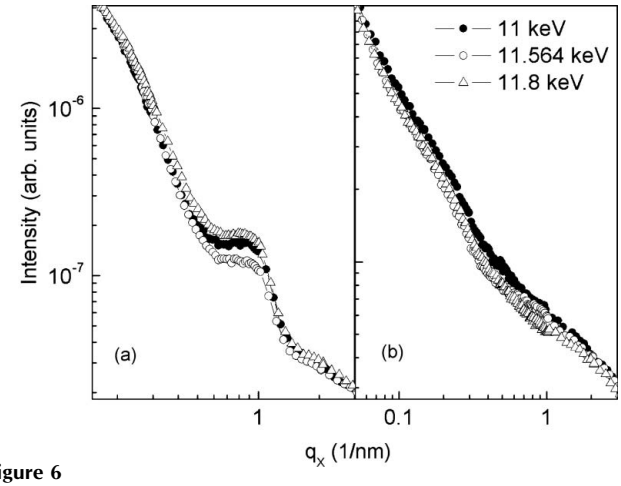

Figure 6
GISAXS spectra of monolayer FePt nanoparticles with an Au overlayer (*a*) before annealing and (*b*) after annealing at 1073 K for 1 h.

Fig. 6 shows the results of anomalous GISAXS of the FePt nanoparticle monolayer on the functional APTS substrate with Au coverlayer before annealing and after annealing. After adding Au as a coverlayer, the Au layer might cover the surface of FePt nanoparticles and remain a similar shape. From the fitting results, the particles remain intact in the Au matrix before the high-temperature annealing. After the 1073 K annealing process for 1 h, a significant feature peak at Q between 0.6 to 1 (nm^{-1}) had disappeared (see Fig. 6), which might indicate that the surface morphology became more flat and smooth. Fig. 7 shows the subtraction of two SAXS curves measured at two different energies E_1 (11.2 keV) and E_2 (11.564 keV), together with the simulation result to describe the scattering curves. The averaged radius R_0 of particles is changed

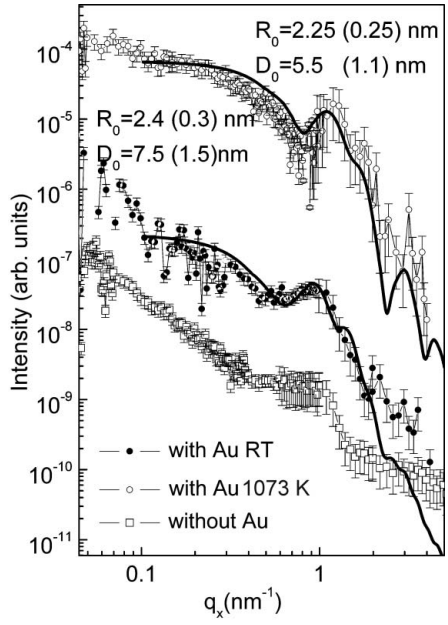

Figure 7
The subtraction of two SAXS curves measured at two different energies E_1 (11.2 keV) and E_2 (11.564 keV) together with the simulation results. The spectra show the morphology with the monolayer of the FePt system without an Au coverlayer before annealing (open square), with an Au coverlayer system before annealing (solid circle) and after the 1073 K annealing process (open circle).

insignificantly (from 2.4 ± 0.3 nm to 2.25 ± 0.25 nm) within the error bars after the annealing process. But the mean distance D_0 (the distance from the particle surface to the surface of neighbouring particle) is reduced from 7.5 ± 1.5 nm to 5.5 ± 1.1 nm. The closer D_0 distance might be caused by burning away surfactants or the change of the Au morphology as we observed from SEM images. Nevertheless, from the simulation results of anomalous GISAXS, the size of FePt particles remains the same in the Au matrix even when the annealing temperature increases up to 1073 K.

In summary, due to the immiscibility between Au and FePt, Au can be a useful material to keep FePt nanoparticles separated. To prevent the aggregation of FePt nanoparticles during the necessary annealing process, adding an Au overlayer to the top of the FePt monolayer enhances the stability of the FePt nanoparticles. The particle size of monolayer FePt nanoparticles can remain small to fit the ultra-high density demand for the next generation magnetic disk.

This research was supported by the National Science Council of Republic of China, under the contract number of NSC91-2112-M007-059. The authors are grateful to the hospitality of the NSRRC.

References

Guinier, A. (1963). *X-ray Diffraction in Crystals, Imperfect Crystals and Amorphous Bodies*. New York: Dover.
Haubold, H. G., Wang, X. H., Jungbluth, H., Goerigk, G. & Schilling, W. (1996). *J. Mol. Struct.* **383**, 283–289.
Held, G. A., Zeng, H. & Sun, S. (2004). *J. Appl. Phys.* **95**, 1481–1484.
Hindle, F., Fertein, E., Seifert, S., Przygodski, C., Bocquet, R., Douay, M. & Bychkov, E. (2005). *J. Non-Cryst. Solids*, **351**, 2200–2204.
Huang, T. W., Huang, Y. H., Tu, T. H. & Lee, C. H. (2004). *J. Magn. Magn. Mater.* **282**, 127–130.
Huang, T. W., Yu, K. L., Liao, Y. F. & Lee, C. H. (2006). *Colloids and Surfaces A: Physicochemical and Engineering Aspects*, **284–285**, 603–606.
Lee, C.-H., Qiu, C.-Z., Yu, K.-L., Liang, J.-H., Tsai, C.-T. & Lin, M. -Z. (2003). *J. Appl. Cryst.* **36**, 612–614.
Rauscher, M., Paniago, R., Metzger, H., Kovats, Z., Domke, J., Pfannes, H. D., Schulze, J. & Eisele, I. (1999). *J. Appl. Phys.* **86**, 6763–6769.
Sun, S., Anders, S., Thomson, T., Baglin, J. E. E., Toney, M. F., Hamann, H. F., Murray, C. B. & Terris, B. D. (2003). *J. Phys. Chem. B*, **107**, 5419–5425.
Sun, S., Murray, C. B., Weller, D., Folks, L. & Moser, A. (2000). *Science*, **287**, 1989–1992.
Wen, F., Waldöfner, N., Schmidt, W., Angermund, K., Bonnemann, H., Modrow, S., Zinoveva, S., Modrow, H., Hormes, J., Beuermann, L., Rudenkiy, S., Maus-Friedrichs, W., Kempter, V., Vad, T. & Haubold, H. G. (2005). *Eur. J. Inorg. Chem.* pp. 3625–3640.
Yu, A.C.C., Mizuno, M., Sasaki, Y., Inoue, M., Kondo, H., Ohta, I., Djayaprawira, D. & Takahashi, M. (2003). *Appl. Phys. Lett.* **82**, 4352–4355.